

Intermittency transitions to strange nonchaotic attractors in a quasiperiodically driven Duffing oscillator

A. Venkatesan and M. Lakshmanan

Center for Nonlinear Dynamics, Department of Physics, Bharathidasan University, Tiruchirappalli - 620 024, India

A. Prasad and R. Ramaswamy

School of Physical Sciences, Jawaharlal Nehru University, New Delhi - 110 067, India

(October 28, 2018)

Different mechanisms for the creation of strange nonchaotic attractors (SNAs) are studied in a two-frequency parametrically driven Duffing oscillator. We focus on intermittency transitions in particular, and show that SNAs in this system are created through quasiperiodic saddle-node bifurcations (Type-I intermittency) as well as through a quasiperiodic subharmonic bifurcation (Type-III intermittency). The intermittent attractors are characterized via a number of Lyapunov measures including the behavior of the largest nontrivial Lyapunov exponent and its variance as well as through distributions of finite-time Lyapunov exponents. These attractors are ubiquitous in quasiperiodically driven systems; the regions of occurrence of various SNAs are identified in a phase diagram of the Duffing system.

I. INTRODUCTION

Interest in the dynamics of quasiperiodically driven systems has grown in recent years largely due to the existence of novel behavior such as strange nonchaotic dynamics. The initial work of Grebogi *et al.* [1] showed that with quasiperiodic forcing, nonlinear systems could have strange nonchaotic attractors (SNAs), namely attractors with a fractal geometry, but with non-positive Lyapunov exponent. Subsequent studies have dealt with a number of important issues pertaining to theoretical as well as experimental aspects [2–16] of SNAs.

While the existence of SNAs is firmly established, a question that remains interesting is the mechanism or bifurcations through which these are created from regular or chaotic attractors. To date a number of different scenarios have been identified: these include torus doubling to chaos via SNAs [3], fractalization of torus [4], the re-emergence of torus doubling sequence and the birth of SNAs [5], the occurrence of SNAs via blow out bifurcation [6], the appearance of SNAs through Type-I intermittent phenomenon [7], or Type-III intermittency [9], and so on [10–16].

Scenarios for the formation of SNAs often have parallels in scenarios for the formation of chaotic attractors. The most common route to SNAs is the gradual “fractalization” of a torus [4] where an amplitude or phase instability causes the collapse of the torus which progressively gets more and more wrinkled as a parameter in the system changes, eventually becoming a fractal attractor. This is also the least well understood mechanism for the formation of SNAs since there is no apparent bifurcation, unlike the crisis-like torus collision mechanisms identified by Heagy and Hammel [3] and Feudel, Kurths and Pikovsky [11]. In the former instance, a period-doubled torus collides with its unstable parent, while in the latter, a stable and unstable torus collide at a dense set of points, leading to SNAs. The quasiperiodic analogue of a saddle-node bifurcation gives rise to SNAs through the intermittent route [7], with the dynamics exhibiting scaling behavior characteristic of Type-I intermittency [17]. The quasiperiodic subharmonic bifurcation, on the other hand, gives rise to Type-III intermittent SNAs [9], when a torus doubled attractor is interrupted by a subharmonic bifurcation, resulting in the inhibition of torus doubling sequence.

Our prime concern in the present work is to understand how a typical nonlinear system, namely the Duffing oscillator, responds to a quasiperiodic forcing and exhibits different dynamical transitions involving SNAs. In particular, intermittencies through which SNAs are formed have been investigated, besides the standard mechanisms like fractalization and torus collision. Although some of these mechanisms have already been identified in certain maps and continuous systems [3,4,7,8], in order to generalize such dynamical transitions in real physical systems, we undertake our investigation on a damped, two frequency parametrically driven double-well Duffing oscillator [18]

$$\ddot{x} + h\dot{x} - [1 + A(R \cos t + \cos \Omega t)]x + x^3 = 0 \quad (1)$$

which is a well-suited model [19] for buckled beam oscillations. The simplest experimental realization of the above equation, the magnetoelastic ribbon has been extensively studied [18,20], and is the first system where SNAs were observed [14] with Ω chosen to be an irrational number. The existence of several routes to SNAs in Eq. (1) suggests that there may be experimental realizations of different types of SNAs which are deserving of further study; our analysis here is thus of some experimental relevance.

The parametrically driven Duffing oscillator, Eq. (1), is a rich dynamical system, possessing a variety of regular, strange nonchaotic and chaotic attractors. We concentrate on the intermittent transitions to SNAs and the mechanism by which they arise in a range in $(R - h)$ parameter space. (In addition to the intermittency routes mentioned above, Yalçinkaya and Lai [6] have shown that on-off intermittency can also be associated with SNAs created through a blowout bifurcation, when a torus loses its transverse stability [6]. This bifurcation does not occur in the present system in the range of parameters studied.)

SNAs represent dynamics which is intermediate between regular and chaotic motion, and therefore they need to be distinguished from chaotic attractors and quasiperiodic (torus) attractors. There are several quantitative criteria that can be used to determine the strange nonchaotic nature [1–13]. The most direct characterization of SNAs is through the largest Lyapunov exponent (which should be nonpositive) and the existence of a nontrivial fractal structure. We employ these criteria in the present work in order to identify strange nonchaotic behaviour: Lyapunov exponents are calculated in the usual manner [21], and the correlation dimension (calculated through the standard Grassberger—Procaccia algorithm [22]) is used to determine whether or not the attractor is fractal. In addition to the fact that Lyapunov exponents are negative on SNAs, the variance of the Lyapunov exponents on SNAs is also large. (Here, by variance we mean the fluctuations in the measured value of finite-time Lyapunov exponents, as calculated from several realizations of the dynamics; see the Appendix). This quantity also shows characteristic changes across transitions to SNAs (particularly when there are crises) [8].

A host of other properties have been used to characterise SNAs, such as the scaling of spectral features or the “phase sensitivity” [11]. SNAs are characterised by specific signatures in their frequency spectrum wherein they admit a power law relation: $N(\sigma) \sim \sigma^{-\alpha}$, $1 < \alpha < 2$, where the spectral distribution function $N(\sigma)$ is defined as the number of peaks in the Fourier amplitude spectrum larger than some value σ . Another measure [11] is based on the presence of a complicated path between the real and imaginary Fourier amplitudes which reflects the fractal geometry of SNAs.

Finer distinctions among SNAs formed via different mechanisms can be made by use of various measures, e. g. the nature of the variation of the Lyapunov exponents and its variance near the transition values of the control parameter [8], the nature of the bursting and scaling laws in the case of intermittent types SNAs [7], the statistical properties of finite-time Lyapunov exponents [23] and so on.

In the next section, the birth of SNAs associated with the mechanisms mentioned above are discussed. In particular, the transition of a two-frequency quasiperiodic attractor \rightarrow torus doubled orbit \rightarrow SNA (through type-III intermittency) \rightarrow chaos and the transition from chaos \rightarrow SNA (through type-I intermittency) \rightarrow torus, besides the standard ones, are shown to be operative in Eq. (1). In Section-III, a number of Lyapunov measures such as the behaviour of the largest Lyapunov exponent, its fluctuations, the distribution of finite-time Lyapunov exponents are used to characterize the transitions from two-frequency quasiperiodicity to SNAs. Our results are summarized in Section IV.

II. THE PARAMETRICALLY DRIVEN DUFFING OSCILLATOR

For our analysis, Eq. (1) can be rewritten as

$$\dot{x} = y, \tag{2}$$

$$\dot{y} = -hy + [1 + A(R \cos \phi + \cos \theta)]x - x^3, \tag{3}$$

$$\dot{\phi} = 1, \quad \dot{\theta} = \Omega. \tag{4}$$

Note that the three equilibrium points of the system for $A = 0$ correspond to $-x + x^3 = 0$, so that there are two stable fixed points $x_{\pm}^s = \pm 1$ and an unstable fixed point at $x^u = 0$.

Fig. 1(a) is the overall phase diagram for the system with the parameters $A = 0.3, \Omega = \sqrt{5} + 1/2$, fixed, while R and h are varied. The dynamical equations are integrated numerically using a fourth-order Runge-Kutta algorithm with adaptive step size. The dynamical states and transitions among them are characterised through the Lyapunov exponents and its variance as well as a number of different measures. The relevant details of the calculation of Lyapunov exponents and their variance are given in the Appendix.

There are a number of different regions where periodic, chaotic and strange nonchaotic attractors can be found: Figs. 1(b), 1(c) and 1(d) are blow-ups of regions W1, W2 and W3 respectively in Fig. 1(a). The various features indicated in the phase diagram are summarized and the dynamical transitions are elucidated in the following.

The general features of the phase diagram fall into a familiar pattern. Compared to the Duffing oscillator driven by a single frequency (the case of $R = 0$), there are new chaotic regions C1, C2 and C3, and bordering the chaotic regions, one has regions where the attractors are strange and nonchaotic. The different regions where quasiperiodic attractors

can be found are also separated here by regions of chaotic attractors and SNAs. In Fig. 1, the region marked TL contains quasiperiodic attractors that oscillate about all the three equilibrium points, x^u, x_{\pm}^s , while TS denotes a small quasiperiodic orbit which oscillates around one of the stable fixed points alone, depending on the initial conditions. The strip denoted D contains interesting dynamical states, both chaotic attractors and SNAs, between which there are a number of transitions.

SNAs are found in a large number of regions, some of which are marked GF1, GF2, GF3, HH1, HH2, S1 and S3 (based on the scenarios responsible for their creation). It should also be pointed out that boundaries separating different dynamical states are very uneven in this phase diagram, which should be considered representative and schematic. In order to illustrate the fine transitions that take place in certain regions when parameter varies, we also present the Lyapunov spectrum as a function of h for fixed R in Fig. 2. Fuller details are discussed below.

Periodic orbits of the forced system with $R = 0$ become quasiperiodic tori of the system with nonzero R . As R is further increased, these tori typically bifurcate via period doubling. Upon further increase of the parameters, there can be further bifurcations or other transformations of the torus attractors to SNAs.

We first discuss the intermittency routes to SNA that can be observed in this system.

A. Type III intermittency

In some regions in $(R - h)$ space the torus doubling sequence is tamed due to subharmonic bifurcations which lead to the creation of SNAs [9]. We find that a growth of the subharmonic amplitude begins together with a decrease in the size of the fundamental amplitude; such behaviour is characteristic of the so-called Type III intermittency [17,24]. The transition from a period-doubled torus to intermittent SNA takes place in the region marked S3 in Fig. 1. From Figs. 1(a) and 1(c), it can be observed that initially the large quasiperiodic orbit (TL) undergoes a torus doubling bifurcation to the torus attractor denoted 2TL. One would then expect the doubling sequence to continue as in the usual period-doubling cascade, but instead, here the doubling is interrupted by the formation of an intermittent SNA which then finally settles into the chaotic attractor C2 as h is increased.

To understand the mechanism of the interruption of the doubling cascade consider a specific parameter value of $R = 0.47$ while h is varied [see Figs. 2(a,b)]. For $h = 0.08$, the attractor is a two-frequency torus, but beyond this, further period doubling of doubled torus does not take place. Instead, a new dynamical behaviour, namely intermittent phenomenon starts appearing at $h = h_c = 0.088689$. This transition is clearly illustrated in Figs. 3 where we note in the $(x, \phi \bmod 4\pi)^1$ plane that the amplitude of one of the components increases while the amplitude of the other component decreases when a transition from doubled torus to intermittent phenomenon takes place. To exemplify this transition further in the Fourier spectrum, it has been identified that the amplitude of the subharmonic component (W2/2) increases while the amplitude of fundamental component (W2) *decreases* during this transition (see Figs. 3). This suggests that the birth of the intermittent SNA is through a quasiperiodic analogue of the subharmonic bifurcation. At this transition, the amplitude variation loses its regularity (Figs. 3) and a burst appears in the regular phase. This behaviour repeats as time increases as observed in the usual intermittent scenario [17,24]. Also, the duration of the laminar phases (namely the quasiperiodic orbit) is random. At the intermittent transition the distinctive signature is an abrupt change in the Lyapunov exponent as well as in its variance as a function of h , as shown in Fig. 4(a,b). This type of SNA occurs in the region $0.088689 < h < 0.088962$. On further increase of the value of h from $h = 0.088963$, we find the emergence of a chaotic attractor (C2) shown in Fig. 3(d), which though visibly similar to the SNA [see Fig. 3(c)] has a positive Lyapunov exponent.

To confirm further that the SNA attractor, Fig. 3(c), is associated with standard type-III intermittent dynamics, we plot the frequency of laminar periods of duration τ , namely $N(\tau)$ in Fig. 4(c). This obeys the scaling [24,25]

$$N(\tau) \sim \left\{ \frac{\exp(-4\epsilon\tau)}{[1 - \exp(-4\epsilon\tau)]} \right\}^{0.5}. \quad (5)$$

We find $\epsilon = 0.009 \pm 0.0003$ to give a best fit for the present data.

¹The various bifurcations and different routes to SNAs can be easily identified by displaying ϕ modulo 4π instead of modulo 2π [19].

B. Type I intermittency

On the right edge of the chaotic region C3, there is a transition from a chaotic attractor to a SNA and then to a quasiperiodic torus, TS. This transition proceeds via Type-I intermittency [7] in the region marked S1 in Fig. 1(a).

Consider the specific parameter value $R = 0.35$ and vary h ; for $h = 0.1907$, the attractor is chaotic [Fig. 5(a)], and as h is increased to $h = 0.190833$, the chaotic attractor transforms to an SNA shown in Fig. 5(b). On increasing the value of h further, an intermittent transition from the SNA to a torus as shown in Fig. 5(c) occurs at $h_c = 0.19088564\dots$. At this transition, the abrupt changes in the Lyapunov exponent as well as its variance [Fig. 6(a,b)] shows the characteristic signature of the intermittent route to SNA as in the Type-III case discussed above. Here the SNA, hopping between the two wells of the system, transforms to the small quasiperiodic torus TS which oscillates in one of the wells as in the case of periodically driven Duffing oscillator [18]. Also, the plot between the number of laminar periods $N(\tau)$ and the period length τ [shown in Fig. 6(c)] indicates that after an initial steep decay there is a slight hump and then a fall off to a small value of $N(\tau)$. It also obeys the relation [24,26]

$$N(\tau) \sim \frac{\epsilon}{2c} \left\{ \tau + \tan \left[\arctan \left(\frac{c}{\sqrt{\frac{\epsilon}{u}}} \right) - \tau \sqrt{\epsilon u} \right] - \arctan \left(\frac{c}{\sqrt{\frac{\epsilon}{u}}} \right) \tau - \tau^2 \sqrt{\frac{\epsilon}{u}} \right\}, \quad (6)$$

where c is the maximum value of $x(t)$, $u = 5.0$ and $\epsilon = 0.0003 \pm +0.00002$.

C. Other routes to SNAs

In addition to the intermittency routes discussed above, the Duffing system has the usual scenarios of torus collision as well as fractalization. The details are as follows.

1. Torus collision

Torus collisions—the route identified by Heagy and Hammel [3]—are denoted HH in Fig. 1. In this scenario, a period- 2^n torus attractor gets wrinkled and upon collision with its parent unstable 2^{n-1} torus, a 2^{n-1} -band SNA is formed. Such a route has been identified in two different regions (HH1 and HH2) of the present system; the resulting SNAs have somewhat different morphologies.

To exemplify the nature of this transition, let us fix the parameter R at 0.3 while h is varied. For $h=0.19$, one finds the presence of a small quasiperiodic attractor which is denoted as TS in Fig. 1, but by $h=0.185$, the attractor undergoes a torus doubling bifurcation and the corresponding region is denoted as 2TS in Fig. 1. When h is decreased further, the two strands of the doubled attractor begin to wrinkle at $h \approx 0.184$ [Fig. 7(a)], and lose continuity when $h \approx 0.181$, resulting in a fractal attractor as shown in Fig. 7(b). The strange nonchaotic [the Lyapunov exponent is negative as seen in Fig. 8(a)] attractor is thus born at the collision of a stable period doubled torus 2TS and its unstable parent TS. Furthermore, this is a one band SNA, as is clearly depicted in Figs. 7, in which prior to the collision, the dynamics in the $(x, \phi \bmod 2\pi)$ plane corresponds to the two branches [Fig. 7a(i)] while it corresponds to a simple curve in the $(x, \phi \bmod 4\pi)$ plane [Fig. 7a(ii)]. However after the collision the dynamics now goes over all of the attractor in both cases of $(x, \phi \bmod 2\pi)$ [Fig. 7b(i)] and $(x, \phi \bmod 4\pi)$ plane [Fig. 7b(ii)].

The Lyapunov exponent also shows distinct change in its behaviour for this type of transition. Fig. 8(a) is a plot of the maximal Lyapunov exponent as a function of h for a fixed value of $R = 0.3$. In the neighborhood of h_c , Λ varies smoothly in the torus region but in the SNA phase the variation is irregular and the crossover between these two behaviours is abrupt. It is also possible to identify the transition point from the examination of the variance in Λ [which increases significantly on the SNA as shown in Fig. 8(b)].

Similar behaviour has also been observed in the region denoted HH2, for $0.37 < R < 0.5$ and $0.11 < h < 0.16$, where the large period-doubled torus (2TL) becomes wrinkled and then interacts with its unstable parent torus leading to the creation of a one band SNA.

2. Fractalization

The process of fractalization [4], whereby a torus continuously deforms and wrinkles to form a SNA can be seen in regions marked GF1–3 in Fig. 1. The qualitative (geometric) structure of the attractors remains more or less the same during the process, unlike the intermittency routes or like the torus collision route discussed in the previous

subsections. In this route, a period- 2^n torus becomes wrinkled and then the wrinkled attractor gradually loses its smoothness and forms a 2^n -band SNA.

This transition can take place both as a function of increasing or decreasing h in different regions of the parameter space as can be seen in the phase diagram. Consider the case $R = 0.47$, with varying h . For $h = 0.05$, the attractor is chaotic [the Lyapunov exponent (see Fig. 2) is positive]. As h is increased to 0.0558, one obtains the attractor shown in Fig. 9(a) which is morphologically similar to the chaotic attractor, but as it has a negative Lyapunov exponent (Fig. 2) it is in fact an SNA. On increasing h to 0.065, the attractor loses its fractal character, becoming a (wrinkled) large quasiperiodic orbit [see Fig. 9(b)]. The Lyapunov exponent (Λ) and its variance (σ) do not show any specific signature as in the case of the intermittent SNA or HH SNA [see Fig. 10(a)].

There are a variety of transitions involving fractalization in the phase diagram. On increasing h to 0.072, along $R = 0.47$ in the GF2 region, the wrinkled attractor again loses its continuity and ultimately approaches a fractal attractor [see Figs. 9(c,d)], getting considerably more wrinkled with increasing h . Beyond $h = 0.0725$, the attractor becomes a doubled large quasiperiodic orbit with period $2TL$. This transition is illustrated in Figs. 7(c,d) (see also Fig. 2) in which the $2TL$ orbit has two bifurcated strands of length 2π for $x > 0$ which are actually a single strand of length 4π . However if one looks in the reverse direction of h , one can note that as the $2TL$ orbit loses its smoothness and develops a fractal nature, the dynamics in the $(x, \phi \text{ modulo } 2\pi)$ plane and $(x, \phi \text{ modulo } 4\pi)$ plane are geometrically the same as in the case of fractalization in the GF1 region described above. The behaviour of the Lyapunov exponent and its variance lack specific signatures at the torus to SNA transitions as demonstrated in Fig. 10(b).

Yet another transition to SNA occurs through gradual fractalization in the region GF3 where a transition from small quasiperiodic attractor (TS) to chaos occurs through torus doubling bifurcation [Figs. 1(a) and 1(d)]. Here the period doubled orbit $2TS$ gets fractalized, leading to the formation of the 2-band SNAs when h is decreased from higher values [see Fig. 1(d)] and the phenomenon is similar to what has been discussed above.

D. Transition between different SNAs

Previous subsections have enumerated the several ways through which SNAs are created from torus attractors. These processes include transitions such as $\dots nT \leftrightarrow n \text{ band SNA} \leftrightarrow \text{chaos}$, $\dots 2^n T \leftrightarrow 2^{n-1} \text{ band SNA} \leftrightarrow \text{chaos}$, etc. One might also observe from the $(R - h)$ phase diagram, Figs. 1 that there are regions where transitions from one type of SNA to another type can occur. Particularly, one may note that transitions occur between (GF2 and S3), (S3 and HH2), (S1 and HH1), and (HH1 and GF3). On closer scrutiny, we find that there exists a narrow range of chaotic motion between the GF2 and S3 as well as the S3 and HH2 regions, while $2TS/TS$ attractors intervene in between S1 and HH1. That is, the transition between S3 and HH2 regions corresponds to: $\dots n \text{ band SNA} \leftrightarrow n \text{ band chaos} \leftrightarrow n \text{ band SNAs} \dots$ and between the regions GF2 and S3 corresponds to: $\dots n \text{ band SNAs} \leftrightarrow n \text{ band chaos} \leftrightarrow \frac{n}{2} \text{ band chaos} \leftrightarrow \frac{n}{2} \text{ band SNAs}$. However in the transition region between GF3 and HH1, see Fig. 1(d), there is band-merging, namely a transition from n -band SNA to $n/2$ -band SNA. This transition [27] is analogous to the phenomenon of reverse bifurcation or band merging bifurcations occurring in chaotic systems, though here the dynamics remains nonchaotic and strange during the transition. Such phenomena have been identified in the driven Henon and circle maps and also in the logistic map [8,13,27]. In the present case we find that as the parameter passes through critical values, the torus doubled attractor does not collide in the GF3 region when undergoing fractalization, whereas it does collide in the HH1 region, thereby leading to a transition from one type of SNA to another (See Fig. 11).

III. PROBABILITY DISTRIBUTIONS OF FINITE-TIME LYAPUNOV EXPONENTS

Owing to the underlying fractal structure, trajectories on a SNA can be locally unstable: finite-time Lyapunov exponents can be positive although the global (or asymptotic) Lyapunov exponent is nonpositive.

As described in the Appendix, we obtain the distribution of finite time Lyapunov exponents, $P(t, \lambda)$ and the variance, through Eq. (A3) or (A4). For most “typical” chaotic motion, a general argument suggests that the density $P(t, \lambda)$ [Eq. (A1)], should be normally distributed [28,29]. On the other hand, for intermittent dynamics, for instance, the system switches between periodic and chaotic states and shows long-range temporal correlations. The probability distribution of these finite-time LEs is asymmetric since it arises from a superposition of two independent densities, each of which is *separately* a Gaussian distribution, centered on a distinct value of the average Lyapunov exponent [30]. On intermittent SNAs, one of the components is a torus with negative or zero Lyapunov exponent, while the other component is chaotic, with average Lyapunov exponent being positive. Finite stretches of intermittent dynamics involve both kinds of motion, and therefore the density of finite-time LEs for intermittency usually results in a stretched exponential tail [30] and in a markedly asymmetric distribution for $P(t, \lambda)$.

Although in the infinite time limit all distributions will go to a δ -function (see Eq. (A2)), for finite times, $P(t, \lambda)$ can be very different for SNAs created through different mechanisms [8,23]. In particular, when the dynamics is intermittent [30], the exponential tails in the distribution persist for long times. Shown in Fig. 12(a) are distributions $P(2048, \lambda)$ for the two intermittent transitions discussed here. Both the distributions have an asymmetric tail which extends well into the locally chaotic (*i.e.* Lyapunov exponent $\Lambda > 0$) region, even for such a long time interval. This correlates with enhanced fluctuations in the Lyapunov exponent on intermittent SNAs. On SNAs formed by the fractalization or torus collision mechanisms, in contrast, similar densities are essentially gaussian [23]; these are shown for comparison in Fig. 12(b).

In order to quantify the slow decay of the positive tail in the distribution for intermittent SNAs, we define the fraction of positive local Lyapunov exponents [30] as

$$F_+(t) = \int_0^\infty P(t, \lambda) d\lambda. \quad (7)$$

Clearly, $\lim_{t \rightarrow \infty} F_+(t) \rightarrow 0$. Empirically, it has been found [23,30] that on the intermittent SNA, this quantity shows the large t behaviour

$$F_+(t) \sim t^{-\beta}; \quad (8)$$

we find numerically that the exponents in both the S1 and S3 regions are $\beta \approx 1$ [31]. For the fractalized or Heagy-Hammel SNAs, the approach is exponentially fast,

$$F_+(t) \sim \exp(-\gamma t). \quad (9)$$

Note that in the long-time limit, all distributions will collapse to the Gaussian, so that for very long times, $t \rightarrow \infty$, F_+ will decay exponentially on all SNAs. The exponents β and γ depend strongly on the system parameters.

IV. CONCLUSION

On SNAs, as a consequence of the fractal geometry, stable and unstable regions are interwoven in a complicated manner. Thus, although trajectories with different initial conditions will eventually coincide with each other [32] since there are no positive Lyapunov exponents, they do so in an intermittent fashion, unlike the case of quasiperiodic attractors, converging in the locally stable regions and diverging in the locally unstable regions.

In this paper we have described the transition from quasiperiodic attractors to chaos through different types of SNAs in a prototypical example, namely the two-frequency parametrically driven Duffing oscillator. We have demarcated the different regions in parameter space where these different dynamical states can be located. There are several mechanisms through which SNAs are formed here, two of which appear to be quasiperiodic analogies of intermittency transitions in unforced systems [17]. In addition to these, we also find evidence for the torus collision route to SNA as well as fractalization.

To distinguish among the different mechanisms through which SNAs are born, we examined the manner in which the maximal Lyapunov exponent and its variance changes as a function of the parameters. In addition, we have also examined the distribution of local Lyapunov exponents and found that on different SNAs they have different characteristics. Our analysis confirms that in the intermittent SNAs, the signature of the transition is a discontinuous change in both the maximal Lyapunov exponent and in the variance. Further, the two different intermittency routes are distinguished by their different scaling behaviours. The chaotic component on both types of intermittent SNAs is long lived, giving, as a consequence, a slowly decaying positive tail in $P(N, \lambda)$ and a resulting power-law decay for $F_+(N)$.

Since the driven Duffing system can be experimentally realized in the driven magnetoelastic ribbon the present work can help in identifying different conditions under which SNAs can be found in a typical system. The study of SNAs—from both theoretical and experimental points of view—is in its initial stages and the present study may aid in the realization of different bifurcation routes to SNA in experimental systems.

V. ACKNOWLEDGMENT

This work forms the part of Department of Science and Technology, Government of India research projects to ML and to RR (SP-S2-E07-96). A. V. wishes to acknowledge Council of Scientific and Industrial Research, Government of India, for financial support.

APPENDIX A: FINITE-TIME LYAPUNOV EXPONENTS

The largest Lyapunov exponent Λ which measures the rate of separation of nearby trajectories can be computed via a standard algorithm [21]. This is an asymptotic quantity, and is a long (in principle infinite) time average of the local rate of expansion in phase space. The finite-time or local Lyapunov exponent $\lambda_i(t)$ is defined in an analogous manner [30,33] except that this is computed over a finite time interval, t . The subscript i indexes the segment (that is, in effect, the initial conditions) in which this exponent is evaluated. A given trajectory is thus divided into segments of length t , and in each of these, the local Lyapunov exponent $\lambda_i(t)$ is computed.

As the finite-time Lyapunov exponents depend on the initial conditions, we consider the probability distributions $P(t, \lambda)$, defined as

$$P(t, \lambda)d\lambda \equiv \text{Probability that } \lambda_i(t) \text{ takes a value between } \lambda \text{ and } \lambda + d\lambda. \quad (\text{A1})$$

This distribution is a stationary quantity, and is particularly useful in describing the structure and dynamics of nonuniform attractors [28,29]. In the asymptotic limit $t \rightarrow \infty$, this distribution will collapse to a δ function,

$$P(t, \lambda) \rightarrow \delta(\Lambda - \lambda). \quad (\text{A2})$$

The deviations from this limit for finite times, and the asymptotics, namely the approach to the limit can be very revealing of the underlying dynamics [30].

From this distribution, one can calculate the variance of the Lyapunov exponent Λ as

$$\sigma = \int_{-\infty}^{\infty} (\Lambda - \lambda)^2 P(t, \lambda) d\lambda. \quad (\text{A3})$$

Equivalently, one can obtain the variance as

$$\sigma = \frac{1}{M} \sum_{i=1}^M (\Lambda - \lambda_i(t))^2, \quad (\text{A4})$$

namely from a set of M finite-time Lyapunov exponents. In our numerical calculations in Sec. II, for instance, we take $t = 50$ and $M \cong 10^5$.

- [1] C. Grebogi, E. Ott, S. Pelikan and J. A. Yorke, *Physica D*, **13**, 261 (1984); C. Grebogi, E. Ott, F.J. Romeiras, and J. A. Yorke, *Phys. Rev. A*, **36**, 5365 (1987).
- [2] F. J. Romeiras and E. Ott, *Phys. Rev. A*, **35**, 4404 (1987); F. J. Romeiras, A. Bondeson, E. Ott, T. M. Antonsen Jr. and C. Grebogi, *Physica D*, **26**, 277 (1987); A. Bondeson, E. Ott and T. M. Antonsen Jr., *Phys. Rev. Lett.*, **55**, 2103 (1985); M. Ding, C. Grebogi and E. Ott, *Phys. Rev. A*, **39**, 2593 (1989); M. Ding and J. A. Scott Kelso, *Int. J. Bifurcation and Chaos* **4**, 553 (1994).
- [3] J. F. Heagy and S. M. Hammel, *Physica D*, **70**, 140 (1994).
- [4] K. Kaneko, *Prog. Theor. Phys.* **71**, 140 (1984); T. Nishikawa and K. Kaneko, *Phys. Rev. E*, **54**, 6114 (1996).
- [5] A. Venkatesan and M. Lakshmanan, *Phys. Rev. E*, **55**, 4140 (1997); *Phys. Rev. E*, **58**, 3008 (1998).
- [6] T. Yaçinkaya and Y. C. Lai, *Phys. Rev. Lett.*, **77**, 5040 (1996).
- [7] A. Prasad, V. Mehra and R. Ramaswamy, *Phys. Rev. Lett.*, **79**, 4127 (1997).
- [8] A. Prasad, V. Mehra and R. Ramaswamy, *Phys. Rev. E*, **57**, 1576 (1998).
- [9] A. Venkatesan, K. Murali and M. Lakshmanan, *Phys. Lett. A*, (1999), in press.
- [10] Y. C. Lai, *Phys. Rev. E*, **53**, 57 (1996); Y. C. Lai, U. Feudel and C. Grebogi, *Phys. Rev. E*, **54**, 6114 (1996).
- [11] A. S. Pikovsky and U. Feudel, *J. Phys. A*, **27**, 5209 (1994); A. S. Pikovsky and U. Feudel, *Chaos* **5**, 253 (1995); U. Feudel, J. Kurths and A. S. Pikovsky, *Physica D*, **88**, 176 (1995); S. P. Kuznetsov, A. S. Pikovsky and U. Feudel, *Phys. Rev. E*, **51**, R1629 (1995).
- [12] T. Kapitaniak and J. Wojewoda, *Attractors of Quasiperiodically Forced Systems*, (World Scientific, Singapore, 1993); T. Kapitaniak, *Phys. Rev. E*, **47**, 1408 (1993); T. Kapitaniak and L. O. Chua, *Int. J. Bifurcation and Chaos* **7**, 423 (1997).
- [13] V. S. Anishchensko, T. K. Vadivasova, and O. Sosnovtseva, *Phys. Rev. E*, **53**, 4451 (1996); O. Sosnovtseva, U. Feudel, J. Kurths and A. Pikovsky, *Phys. Lett. A*, **218**, 255 (1996).

- [14] W. L. Ditto, M. L. Spano, H. T. Savage, S. N. Rauseo, J. F. Heagy and E. Ott, Phys. Rev. Lett., **65**, 533 (1990).
- [15] T. Zhou, F. Moss and A. Bulsara Phys. Rev. A, **45**, 5394 (1992).
- [16] W. X. Ding, H. Deutsch, A. Dinklage and C. Wilke, Phys. Rev. E, **55**, 3769 (1997).
- [17] Y. Pomeau and P. Manneville, Commun. Math. Phys. **74**, 189 (1980).
- [18] M. Lakshmanan and K. Murali, *Chaos in Nonlinear Oscillators : Synchronization and Control*, (World Scientific, Singapore, 1996).
- [19] J. F. Heagy and W. L. Ditto, J. Nonlinear Sci. **1**, 423 (1991).
- [20] W. L. Ditto, S. Rauseo, R. Cawley, C. Grebogi, G. H. Hsu, E. Kostelich, E. Ott, H. T. Savage, R. Segnam, M. L. Spano and J. A. Yorke, Phys. Rev. Lett., **63**, 923 (1989); H. T. Savage, W. L. Ditto, P. A. Braza, M. L. Spano and W. C. Spring, J. Appl. Phys. **67**, 5619 (1990); H. T. Savage and M. L. Spano, J. Appl. Phys. **53**, 8002 (1982); H. T. Savage and C. Adler, J. Magn. Mater. **58**, 320 (1986).
- [21] G. Benettin, L. Galgani, and J.-M. Strelcyn, Phys. Rev. A, **14**, 2338 (1976).
- [22] P. Grassberger and I. Procaccia, Physica D, **9**, 189 (1983).
- [23] A. Prasad and R. Ramaswamy, *Finite time Lyapunov exponents on Strange Nonchaotic Attractors*, (LANL Bulletin Board, chaos-dyn/9801021); in *Nonlinear Dynamics: Integrability and Chaos*, Ed. M. Daniel *et al.*, Narosa Publishing Co., New Delhi, 1999, to appear.
- [24] H. G. Schuster, *Deterministic chaos*, (Physik-Verlag, Weinheim, 1984).
- [25] M. Dubois, M. A. Rubio and P. Berge, Phys. Rev. Lett., **51**, 1446 (1983).
- [26] J. E. Hirsch, B. A. Huberman and D. J. Scalapino, Phys. Rev. A, **25**, 519 (1982).
- [27] S. S. Negi, A. Prasad, and R. Ramaswamy, to be published.
- [28] P. Grassberger, R. Badii, and A. Politi, J. Stat. Phys. **51**, 135 (1988).
- [29] E. Ott, *Chaos in dynamical systems*, (Cambridge University Press, Cambridge, 1994).
- [30] A. Prasad and R. Ramaswamy, Phys. Rev. E, **60**, 2761 (1999).
- [31] At $R = 0.45$ and $h = 0.100736782$ (in the S3 region) the exponent β is 1.14 and in the S1 region, at $R = 0.35$ and $h = 0.190865$, the exponent is 0.89.
- [32] R. Ramaswamy, Phys. Rev. E, **56**, 7294 (1997).
- [33] H.D.I. Abarbanel, R. Brown and M.B. Kennel, J. Nonlinear Sci. **1**, 175 (1991).

FIG. 1. Phase diagram for the parametrically driven Duffing oscillator system, Eqs. (2)-(4), in the $(R - h)$ parameter space. Here 2TS and 2TL correspond to torus doubled attractors of small and large quasiperiodic orbits, respectively. GF1, GF2 and GF3 correspond to the regions where the process of gradual fractalization of torus occurs. HH1 and HH2 represent the regions where SNA is created through the Heagy-Hammel route. S1 and S3 denote regions where the SNA appears through Type-I and Type-III intermittencies respectively. C1, C2 and C3 correspond to chaotic attractors. Regions W1, W2 and W3 in Fig. 1(a) are expanded in Figs. 1(b), 1(c) and 1(d), and the inset in Fig. 1(b) illustrates the intertwining of chaotic (C1) and quasiperiodic orbits (TL); the two levels curves correspond to the specific values of the maximal Lyapunov exponent: $\Lambda=0$ (...) and $\Lambda=-0.005$ (---).

FIG. 2. The behaviour of the Lyapunov exponent as a function of h for (a) $R = 0.47$, (b) $R = 0.47$ and (c) $R = 0.4$. Here the notation is the same as in Fig. 1 (Tr stands for transients).

FIG. 3. Projection of the two-frequency attractors of Eqs. (2)-(4) for $R=0.47$, with the Poincaré plot in the (x, ϕ) plane (i) ϕ modulo 2π and (ii) ϕ modulo 4π (iii) power spectrum indicating the transition from chaotic to quasiperiodic attractors via SNA through type-III intermittent mechanism: (a) two frequency doubled quasiperiodic orbit for $h = 0.075$; (b) doubled torus for $h = 0.08$; (c) intermittent SNA for $h = 0.088689$; (d) chaotic attractor for $h = 0.088963$.

FIG. 4. Transition from doubled torus to SNA through type-III intermittent mechanism in the region S3: (a) the behaviour of the Lyapunov exponent (Λ); (b) the variance (σ); (c) Number of laminar periods $N(\tau)$ of duration τ in the case of transition through type-III intermittency.

FIG. 5. Projection of the two-frequency attractors of Eqs. (2)-(4) for $R=0.35$, with the Poincaré plot in the (x, ϕ) plane (i) ϕ modulo 2π and (ii) ϕ modulo 4π indicating the transition from quasiperiodic to chaotic attractors via SNA through type-I intermittency mechanism: (a) chaotic attractor for $h = 0.1907$; (b) intermittent SNA for $h = 0.190833$; (c) torus for $h = 0.1908564$.

FIG. 6. Transition from torus to SNA through type-III intermittent mechanism in the region S3: (a) the behaviour of the Lyapunov exponent (Λ); (b) the variance (σ); (c) Number of laminar periods $N(\tau)$ of duration τ in the case of transition through type-I intermittency.

FIG. 7. Projection of the two-frequency attractors of Eqs. (2)-(4) for $R = 0.3$, with the Poincaré plot in the (x, ϕ) plane (i) ϕ modulo 2π and (ii) ϕ modulo 4π indicating the transition from chaotic to quasiperiodic attractors via SNA through Heagy-Hammel (HH1) mechanism: (a) torus doubled attractor for $h = 0.184$; (b) strange nonchaotic attractor for $h = 0.181$.

FIG. 8. Transition from doubled torus to SNA through Heagy-Hammel mechanism in the region HH1: (a) the behaviour of the Lyapunov exponent (Λ); (b) the variance (σ).

FIG. 9. Projection of the two-frequency attractors of Eqs. (2)-(4) for $R = 0.47$, with the Poincaré plot in the (x, ϕ) plane (i) ϕ modulo 2π and (ii) ϕ modulo 4π indicating the transition from chaotic to quasiperiodic attractors via SNA through fractalization (GF1 and GF2). (a) strange nonchaotic attractor for $h = 0.0558$ (GF1); (b) wrinkled attractor for $h = 0.065$; (c) strange nonchaotic attractor for $h = 0.072$ (GF2); (d) torus doubled attractor for $h = 0.0729$.

FIG. 10. Transition from torus to SNA through Gradual fractalization mechanism indicating (i) the behaviour of the Lyapunov exponent (Λ); (ii) the variance (σ): (a) in the region GF1; (b) in the region GF2.

FIG. 11. Transition from gradual fractalization (GF3 region) type of SNA to Heagy-Hammel (HH1 region) type of SNA for $h = 0.1675$: (a) SNA (GF3 region) for $R = 0.1955$; (b) SNA (GF3 region) for $R = 0.197$; (c) SNA (HH1 region) for $R = 0.1974$; (d) SNA (HH1 region) for $R = 0.203$.

FIG. 12. Distribution of finite-time Lyapunov exponents on SNAs created through (a) Type-III (dashed line) and Type-I intermittency (solid line), with $t = 2048$, and (b) torus collision (the Heagy-Hammel route) (dotted line) and fractalization (solid line). The parameter values are those of Figs. 3(c), 5(b), 7(b) and 11(a) respectively.

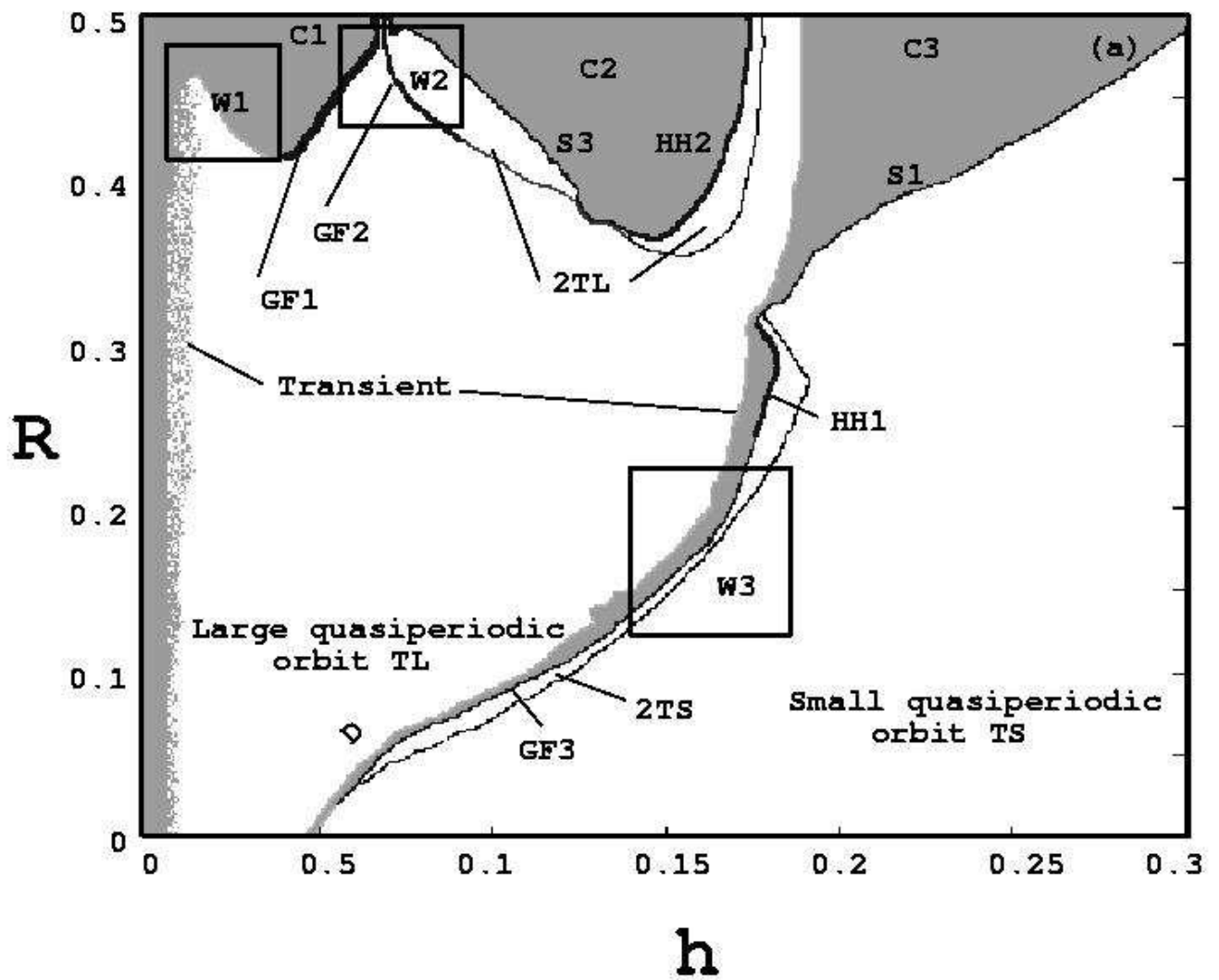


FIG. 1a (A. Venkatesan et al.)

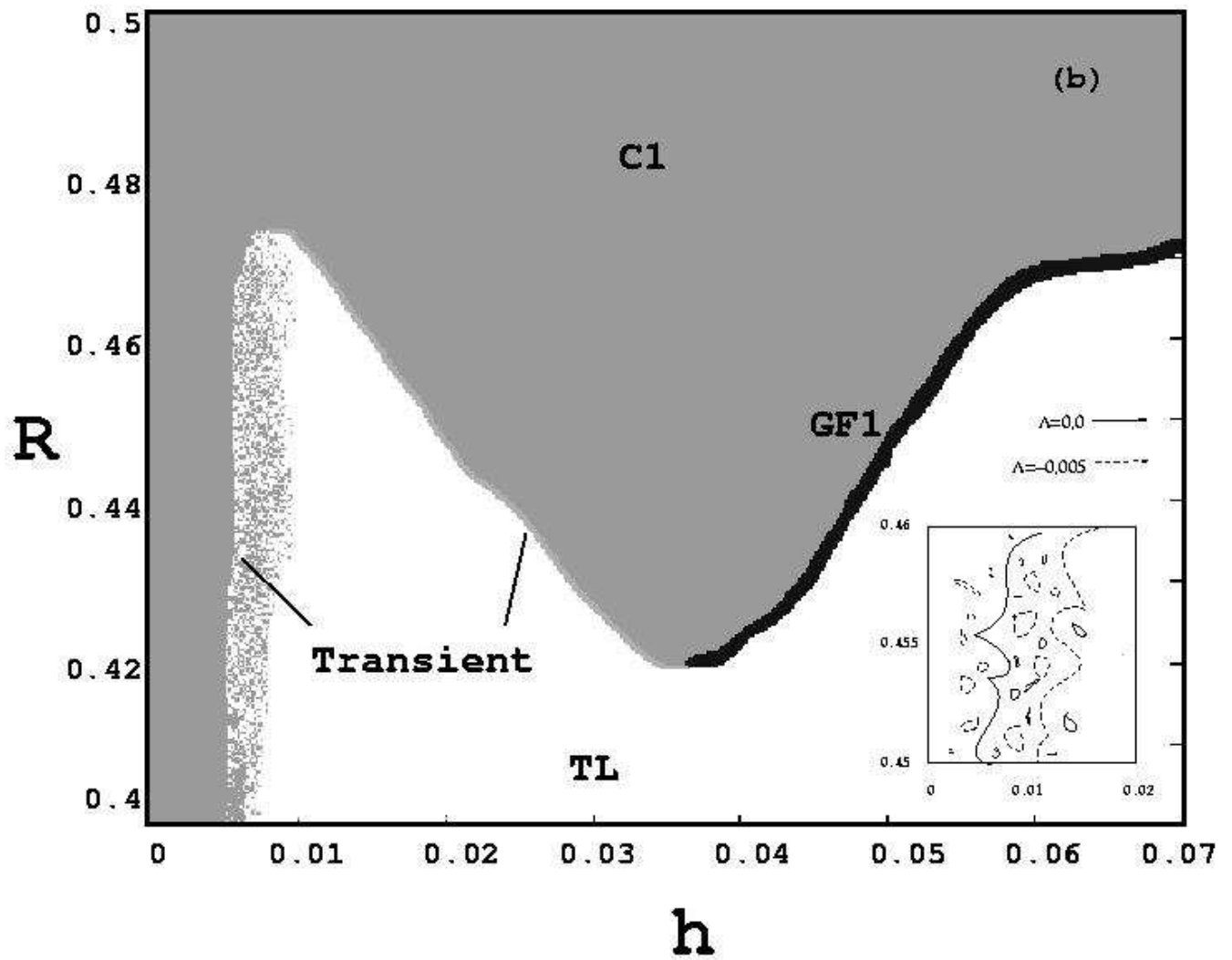


FIG. 1b (A. Venkatesan et al.)

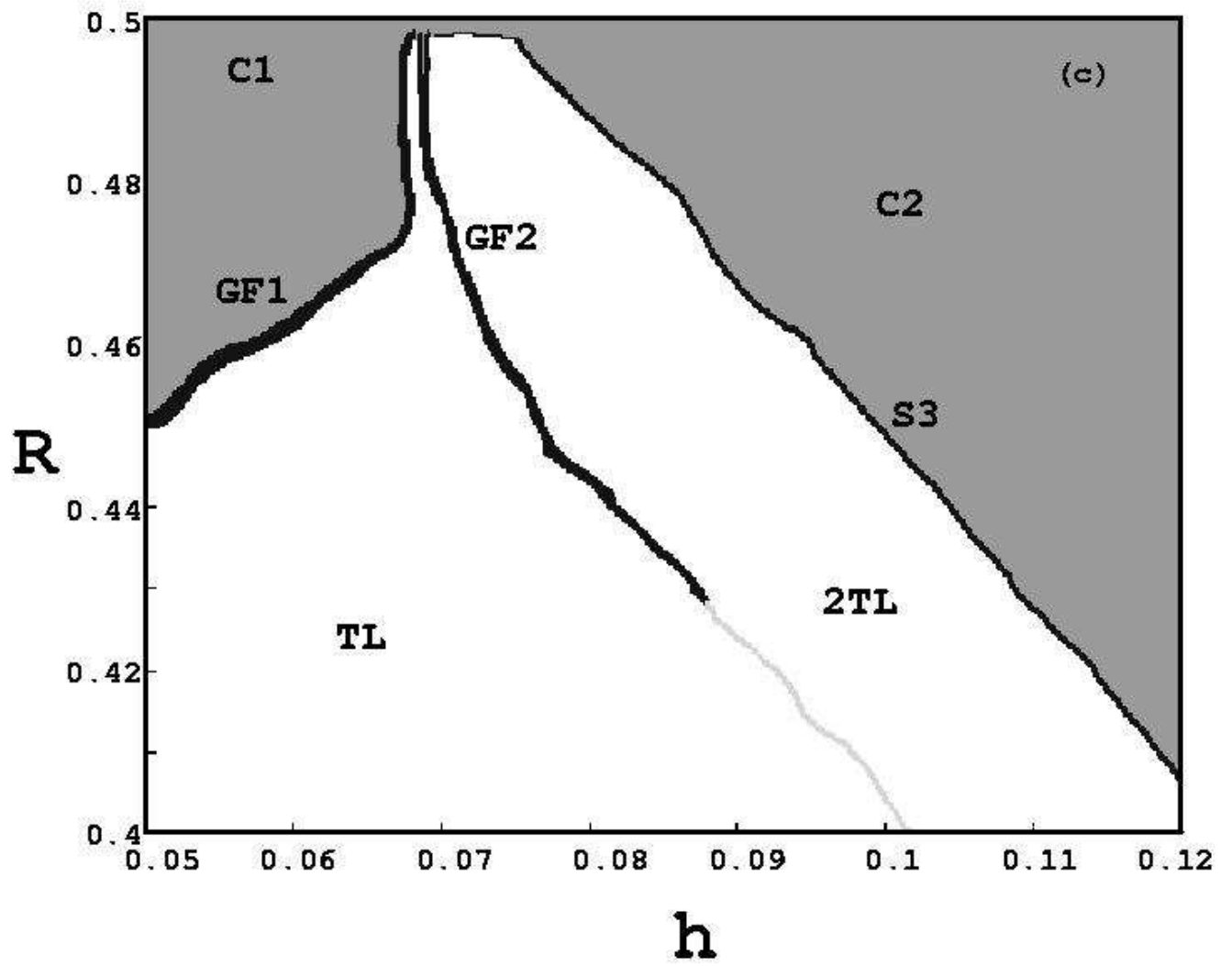


FIG. 1c (A. Venkatesan et al.)

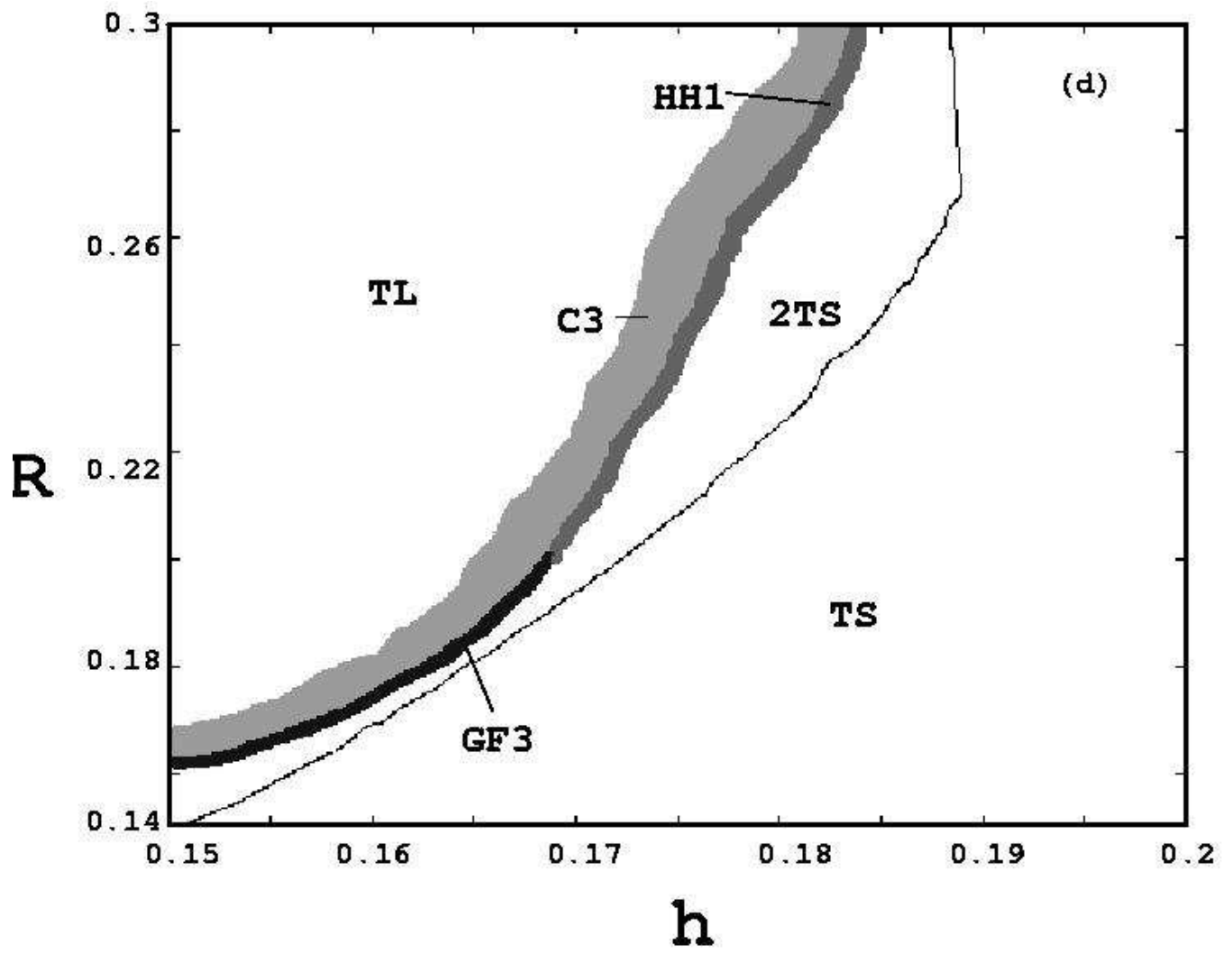


FIG. 1d (A. Venkatesan et al.)

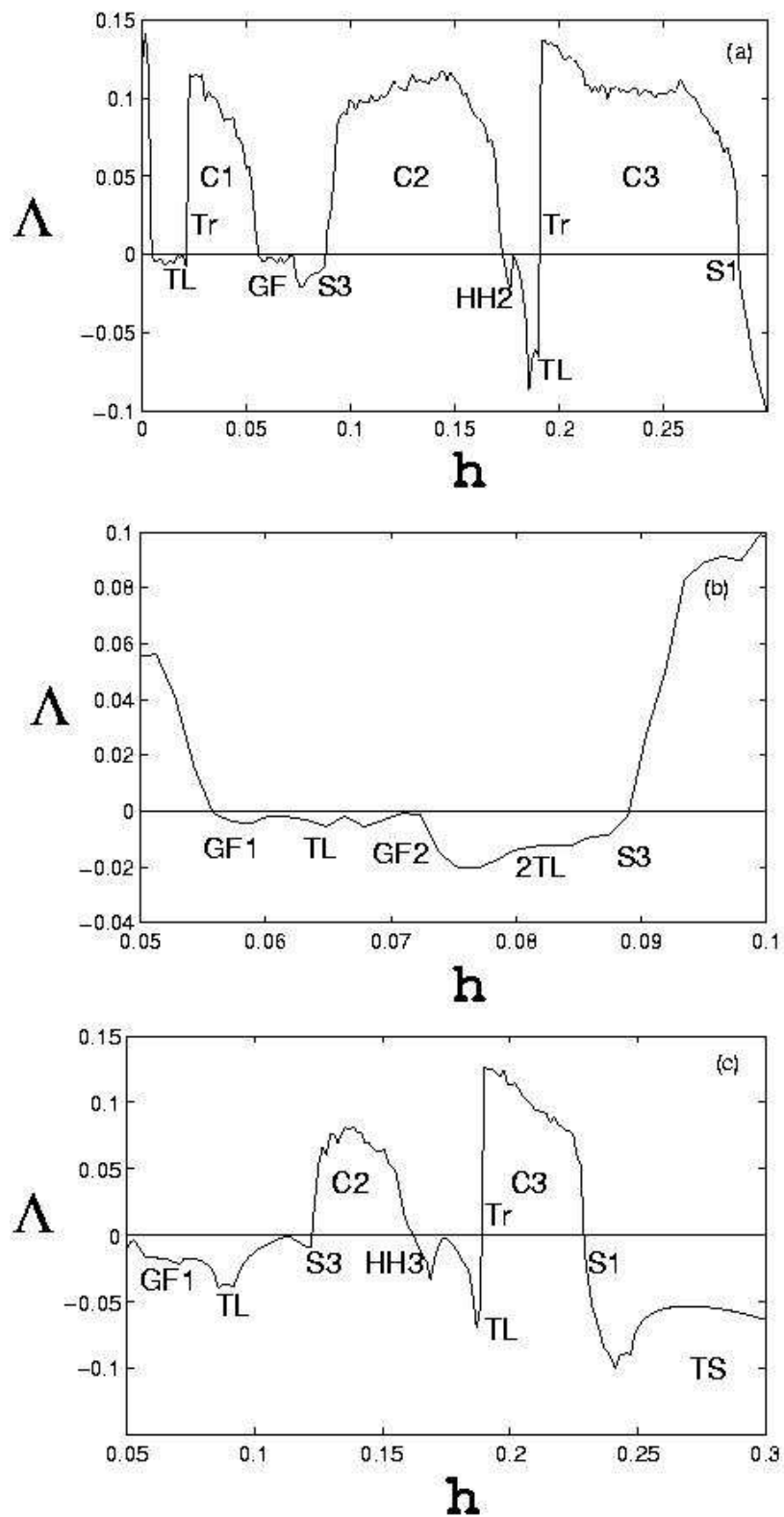


FIG. 2 (A. Venkatesan et al.)

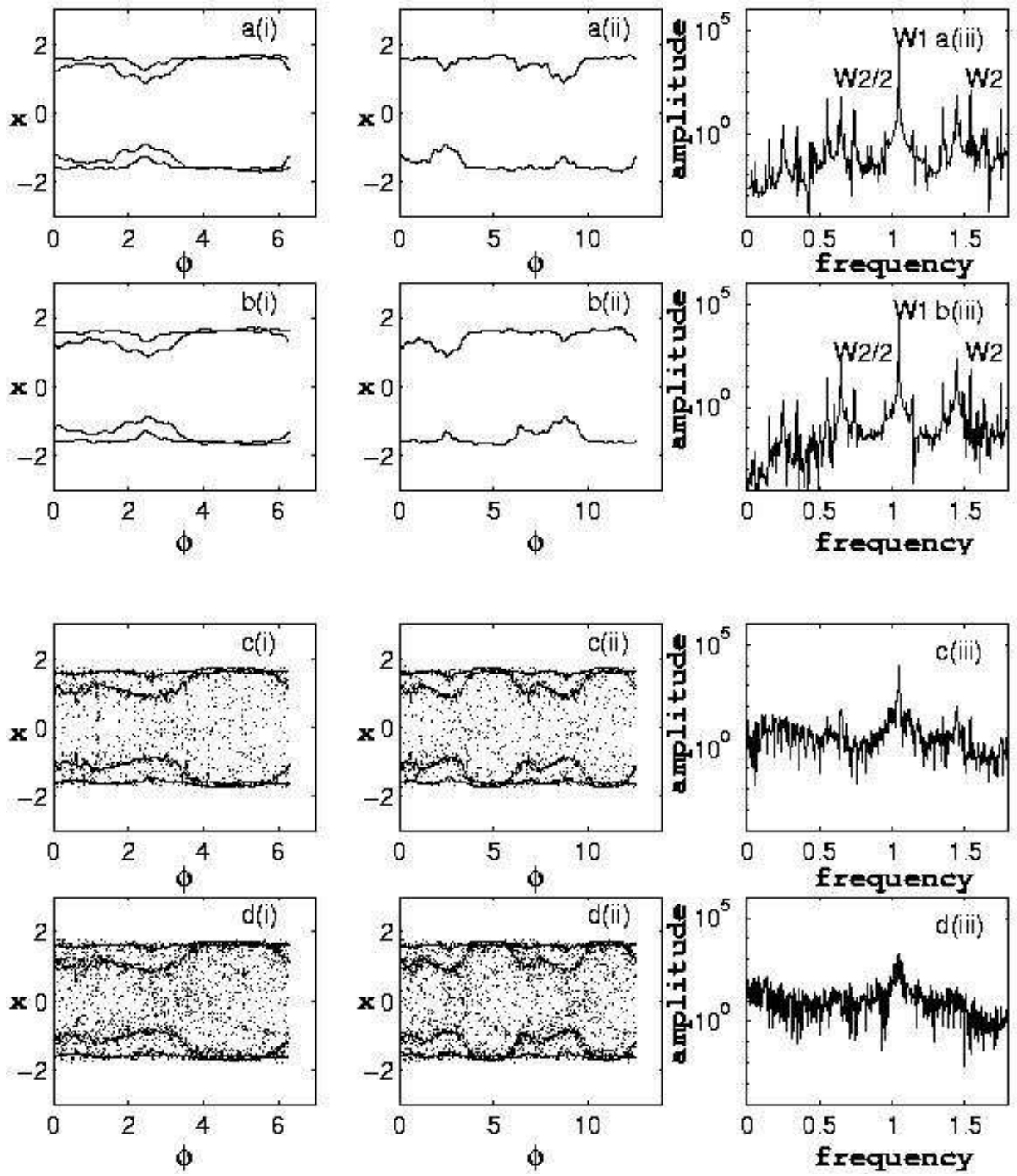


FIG. 3 (A. Venkatesan et al.)

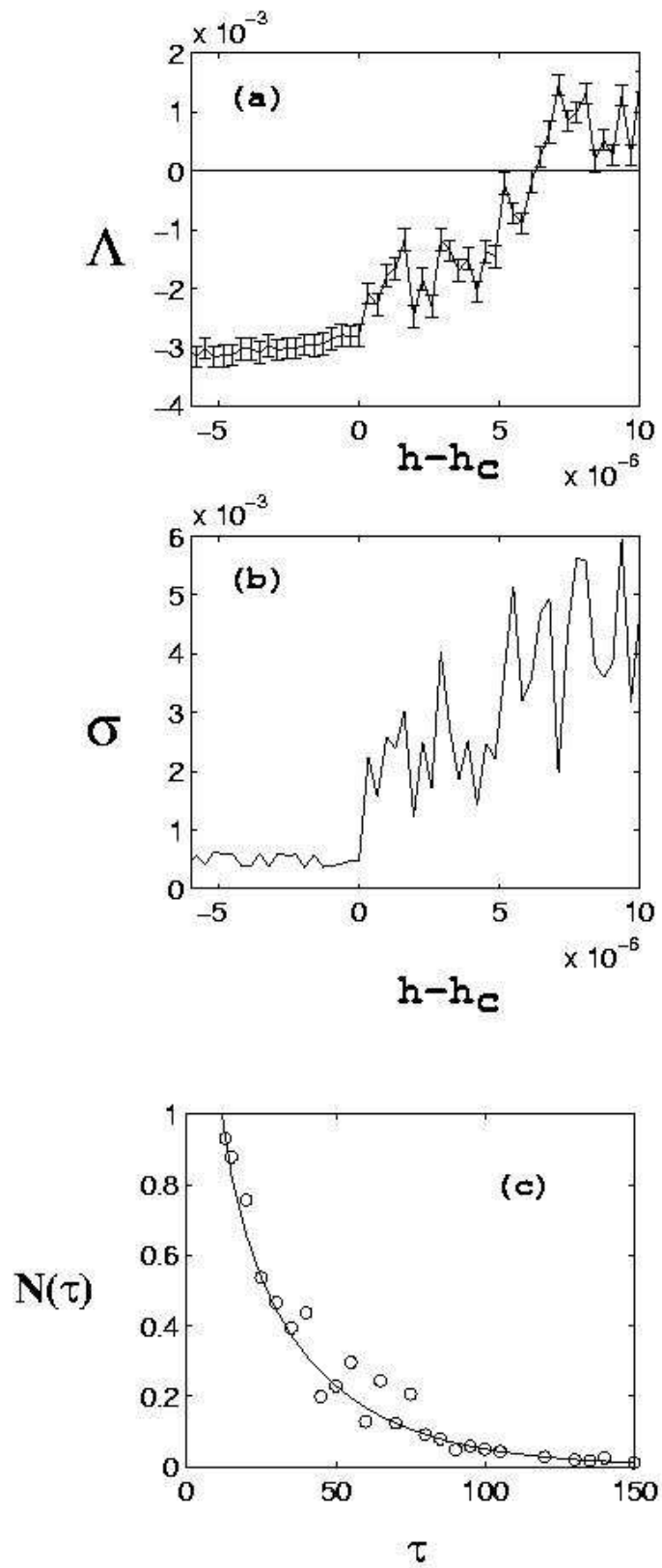


FIG. 4 (A. Venkatesan et al.)

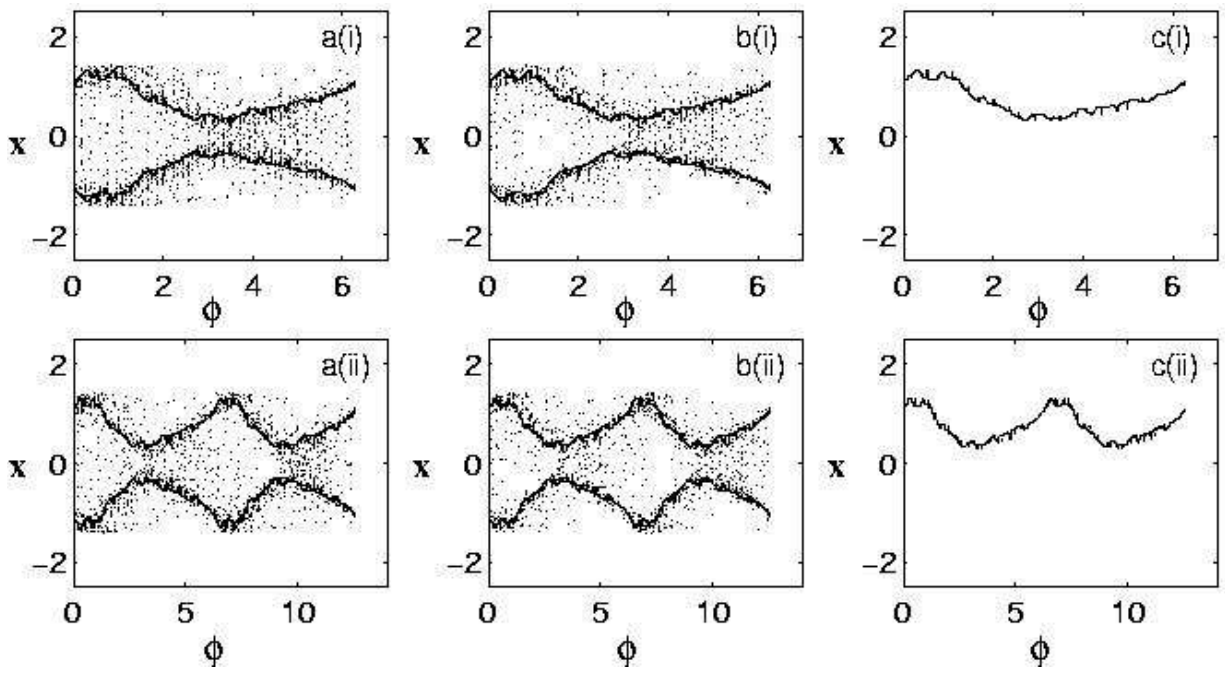


FIG. 5 (A. Venkatesan et al.)

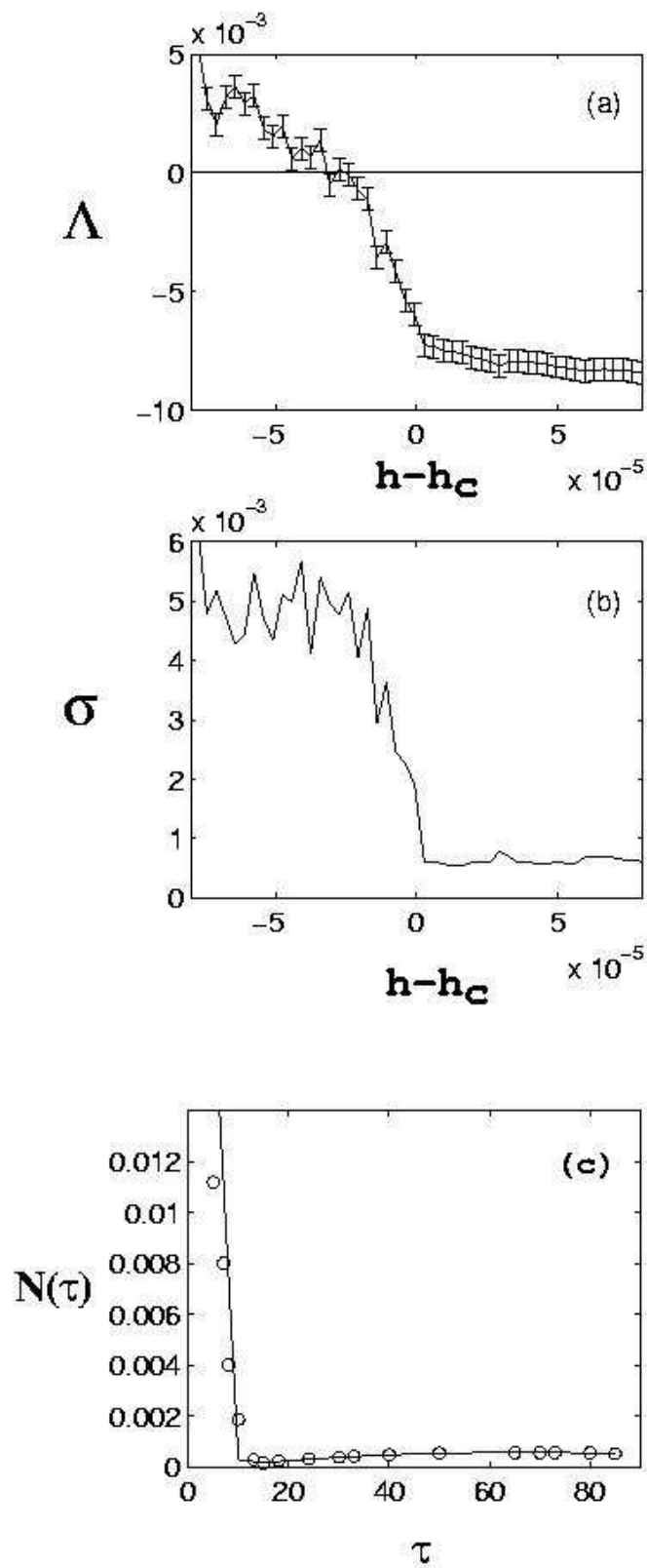


FIG. 6 (A. Venkatesan et al.)

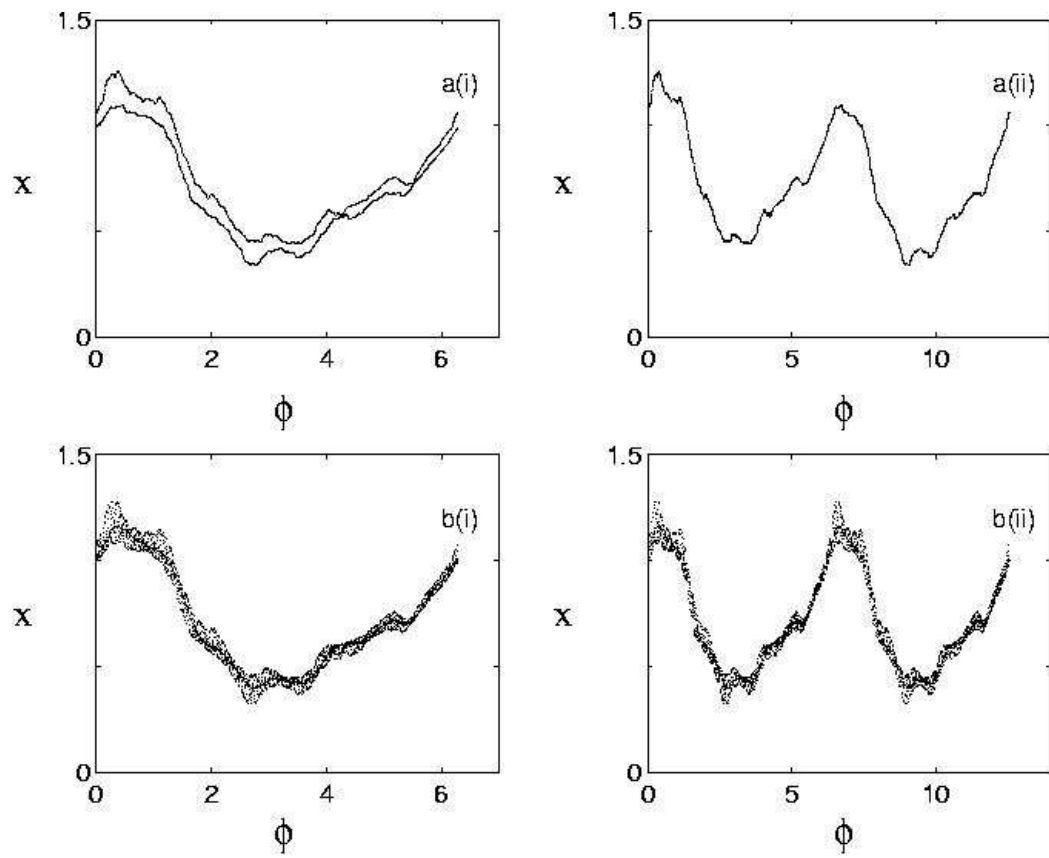


FIG. 7 (A. Venkatesan et al.)

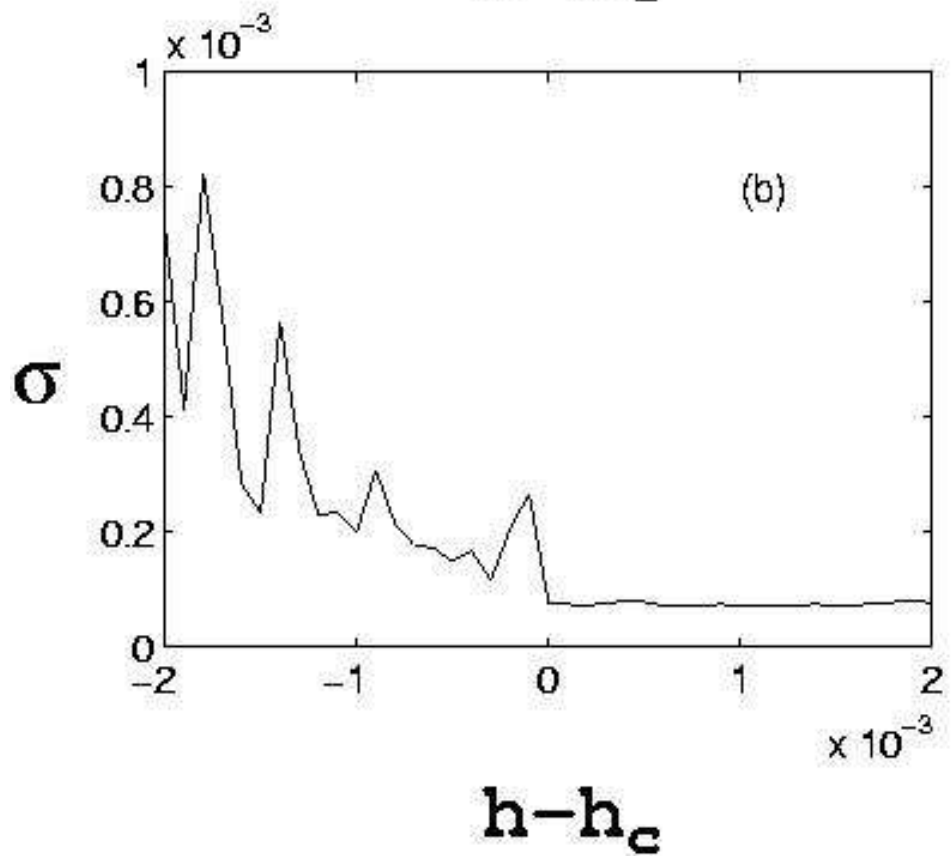
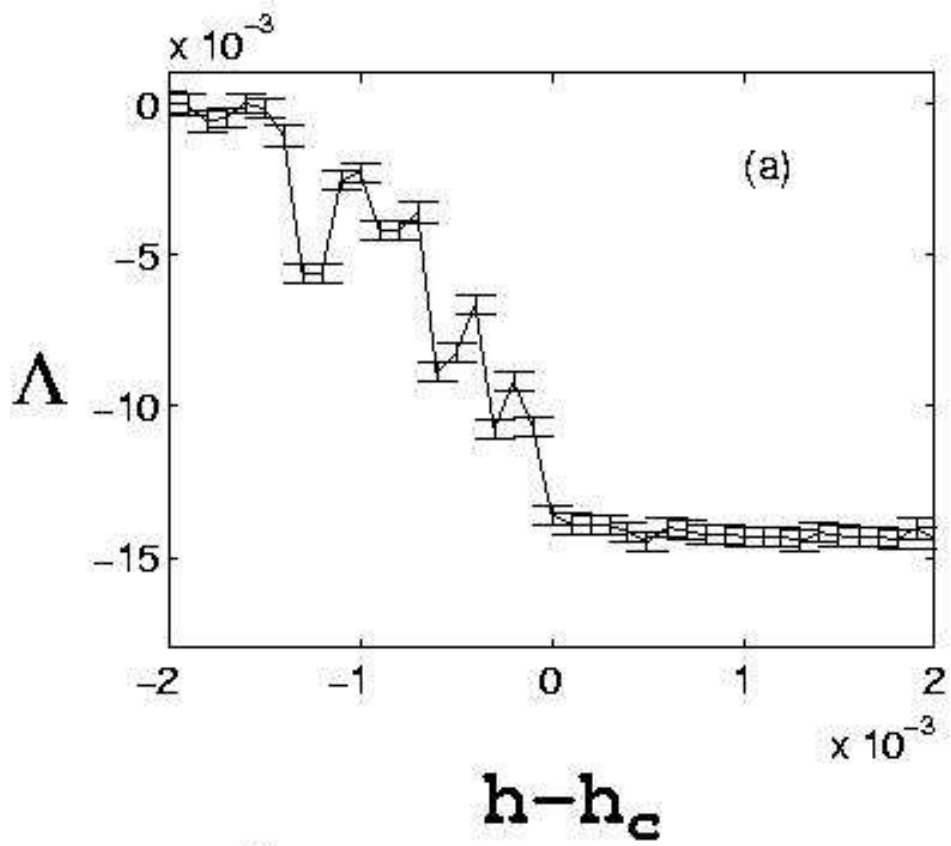


FIG. 8 (A. Venkatesan et al.)

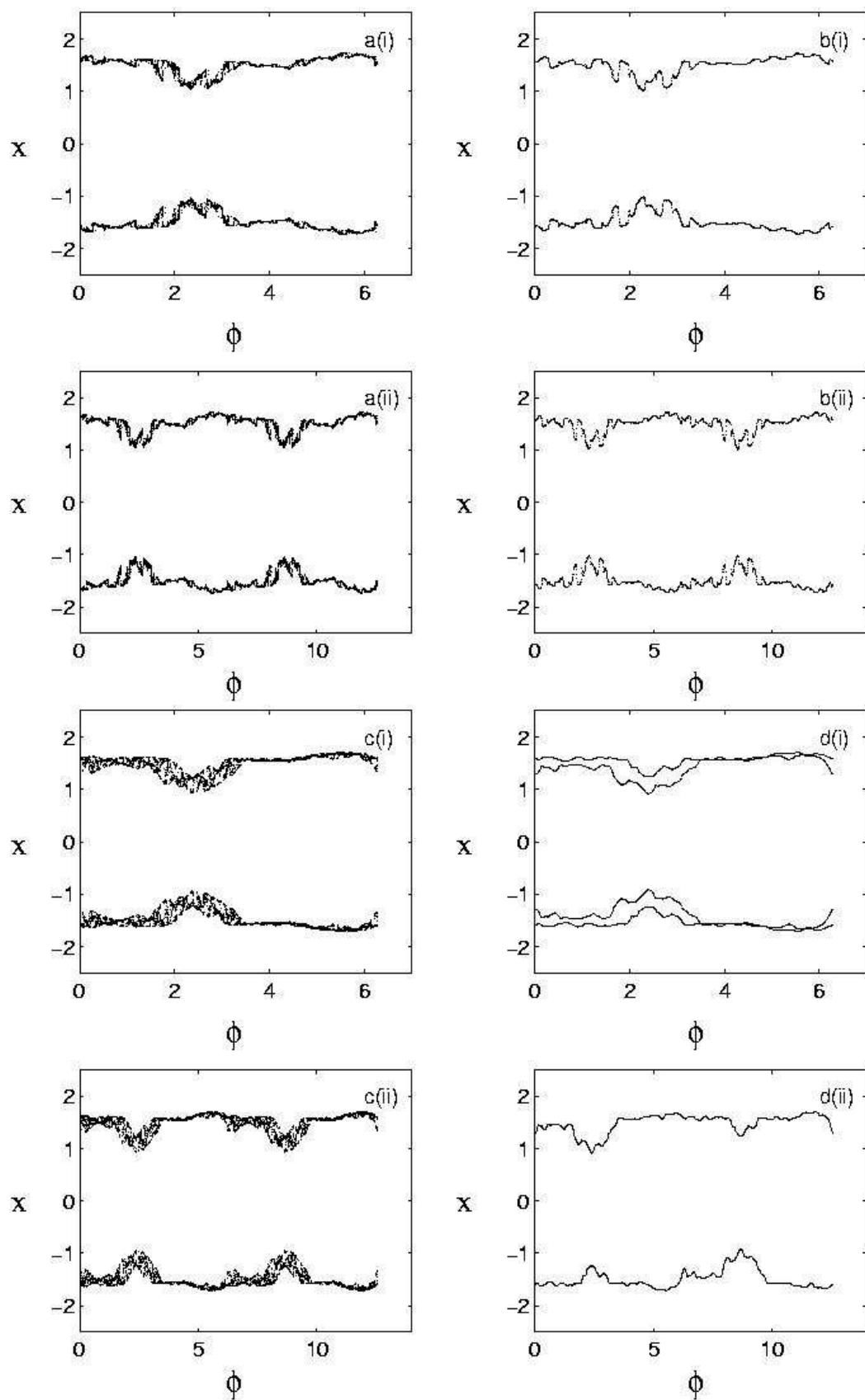


FIG. 9 (A. Venkatesan et al.)

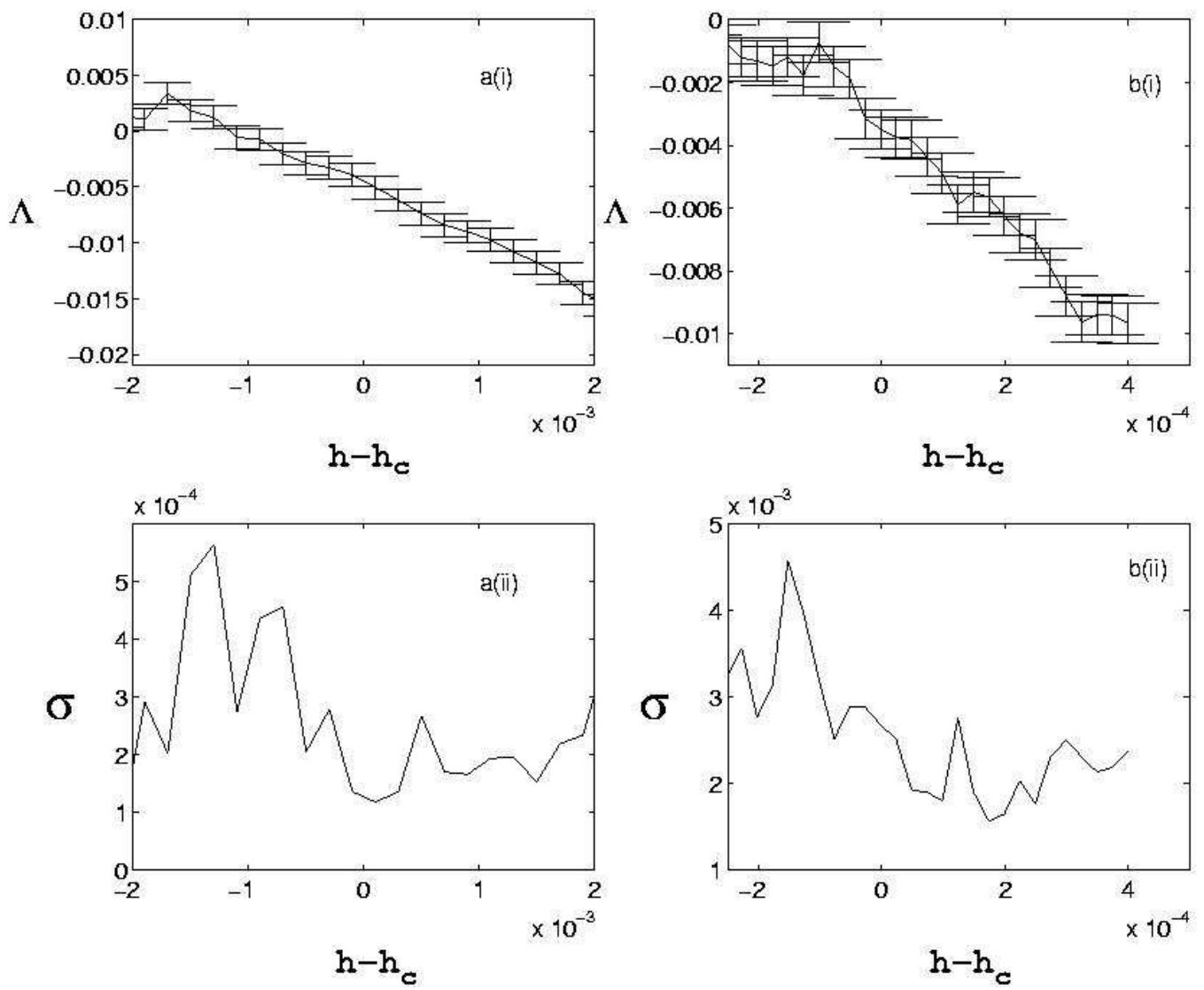


FIG. 10 (A. Venkatesan et al.)

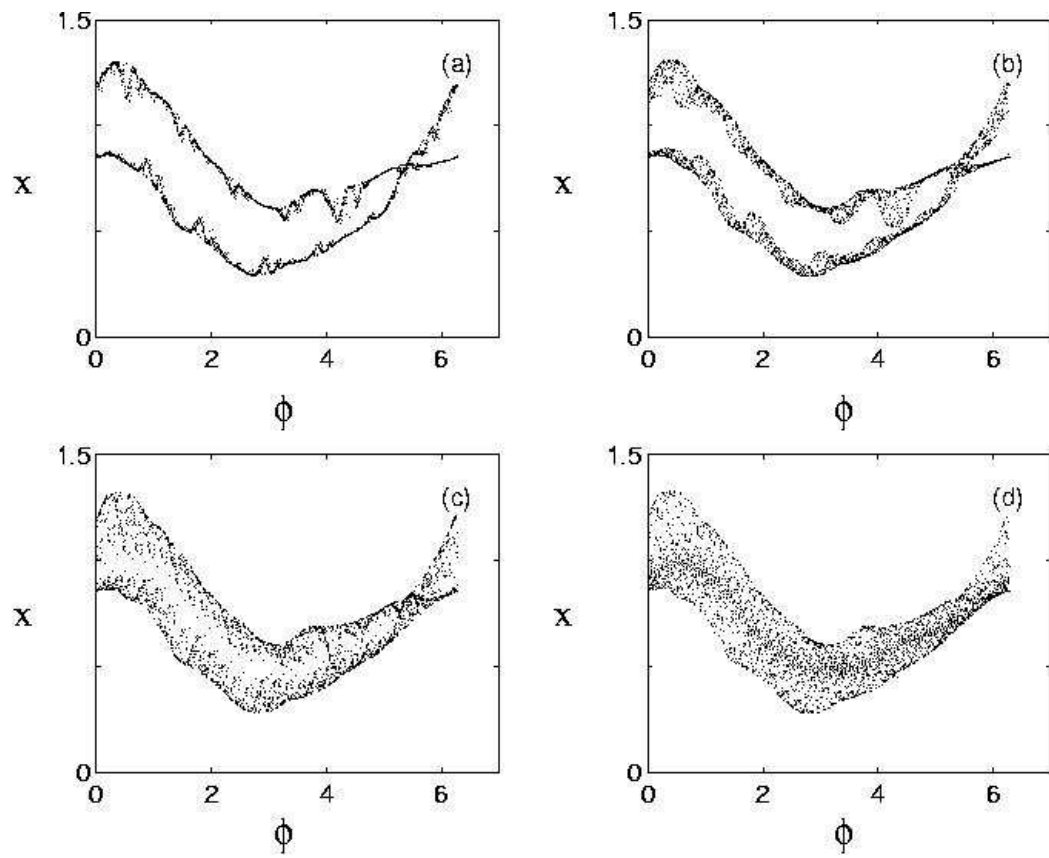


FIG. 11 (A. Venkatesan et al.)

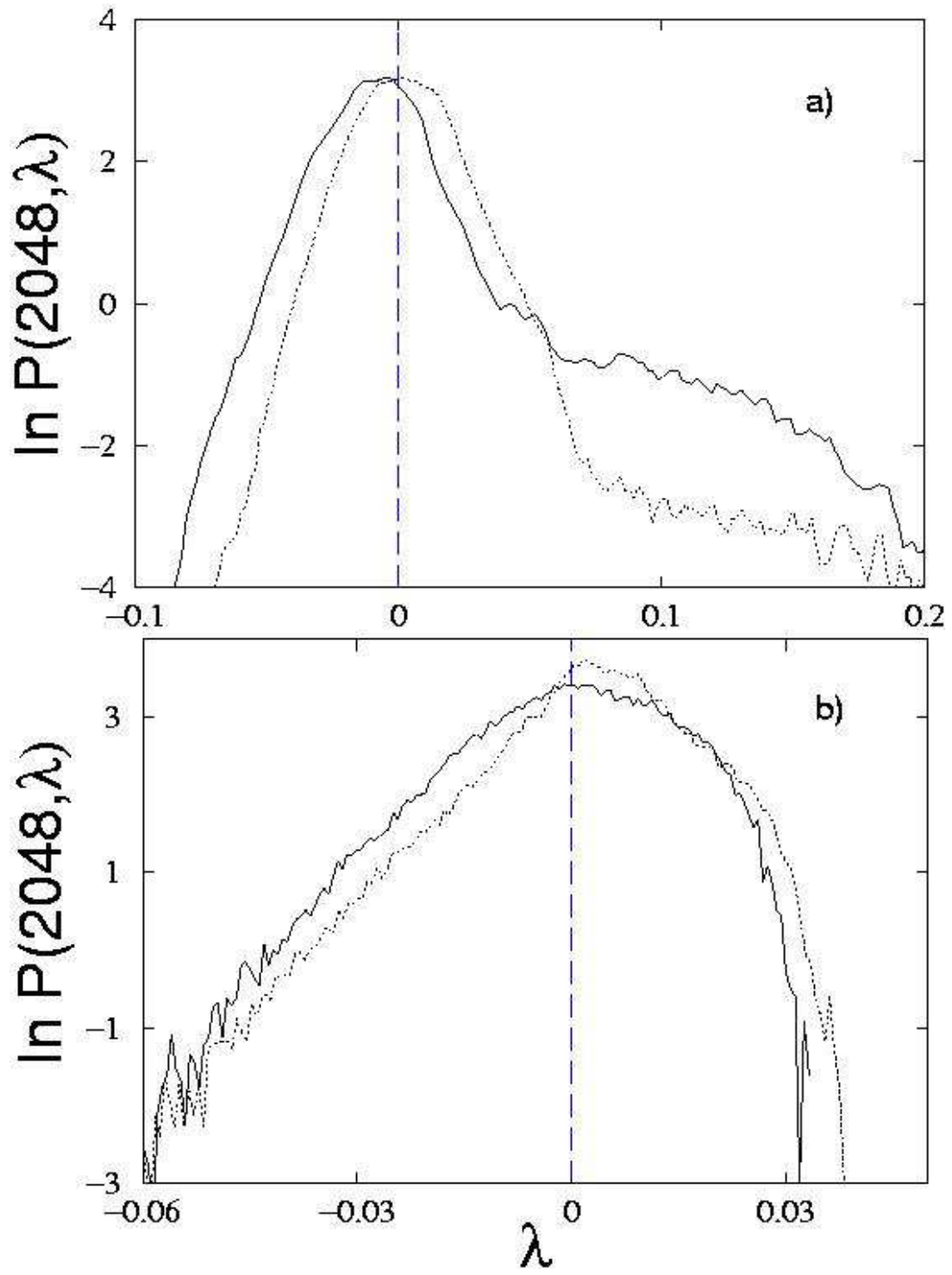


FIG. 12 (A. Venkatesan et al.)